COMSOL CONFERENCE 2020 EUROPE

Enhanced Physics-Based Models for State Estimation of Li-Ion Batteries

Daniel Luder[1], Priscilla Caliandro[1], Andrea Vezzini[1]
[1]BFH Energy Storage Research Centre (ESReC), Bern University of Applied Sciences (BFH), 2560 Nidau, Switzerland

Abstract

Battery models and state estimation algorithms are a key components of todays advanced Battery Management Systems (BMS). Thereby, the battery models are used to estimate non-measurable states in the battery to ensure safety and availability while prolonging its life. This paper focuses on pseudo-2D physics-based battery models namely the Doyle-Fuller-Newman (DFN) model and Single Particle Model (SPM) that are capable to represent battery internal electrochemical states, that are vital for high precision simulation of the battery behavior. A three-step DFN model parameter identification procedure including QR decomposition with column pivoting, microstructure analysis and model optimization is proposed and applied on a commercial 18650 lithium-ion battery. The DFN model is validated with drive cycles as they occur in Electric Vehicles (EV) revealing a RMSE smaller than 18mV on average over the full SOC range. In the end, the DFN model is used to validate a state-space implementation of a SPM with electrolyte dynamics, which can be implemented on an embedded system to estimate battery states in real-time.

Introduction

Batteries are ubiquitous and indispensable in our modern world, enabling a highly connected and mobile society. They are one of the key elements in transforming power generation as well as mobility and transportation to more sustainable and renewable energies. Lithium-ion batteries in particular are widely used due to their high energy and power density and long service life. In recent years these properties have been improved while at the same time the price has been reduced [1]. One of the major challenges for batteries is the accurate electrochemical meaningful estimation of cell internal states. Among these states are the State of Charge (SOC) describing the available charge, the State of Health (SOH) representing the battery lifetime, the State of Power (SOP) describing the available power limitations and the cell impedance. The determination of those states is not as simple as for example in a gasoline powered car, where the content of the fuel tank remains constant over the lifetime and can be measured directly with a fuel level sensor.

A key component of a complete battery system is the Battery Management System (BMS) that monitors all cells within the battery pack and keeps them in a safe state (voltage, current and temperature). In most advanced BMSs, battery models are used in combination with appropriate state estimation algorithms e.g. Kalman filters, to estimate the directly not measurable cell internal states in real-time [2].

The most common cell model for commercial products is based on equivalent circuits (ECM) consisting of voltage sources, resistors, capacitors and hysteresis models. The advantage of this model lies in its easy interpretability, simple parameter identification, robustness against high current changes and low computing power, which is essential for an implementation on an embedded system. A major disadvantage of the ECM is the lack of representation of the electrochemical properties and processes within the cell. These characteristics are particularly important to know whether and to what extent aging processes take place, such as the Solid Electrolyte Interphase (SEI) layer growth [2, p. 282–289] or lithium plating [2, p. 292–294]. In order to prolong battery life, they must be prevented or minimized by suitable control algorithms and strategies.

The Physics-Based Model (PBM) developed by Doyle, Fuller and Newman Model, also known as Doyle-Fuller-Newman (DFN) model, represents all cell-internal electrochemical properties and dynamics [3, 4]. Unfortunately, this model consists of several nonlinear coupled Partial Differential Equations (PDEs), making the model computationally expensive and consequently unsuitable for the implementation on BMSs. Therefore, the DFN can be simplified to the Single Particle Model (SPM) that approximates the porous solid phase of each electrode with a single spherical particle. Further methods exist to simplify the SPM model by neglecting, averaging and fitting properties and processes while maintaining the electrolyte dynamics [5-7].

In ideal case the cell model can be represented as reduced order state-space model enabling the combination with an Extended Kalman Filter (EKF) for accurate state estimation [8]. Moreover, the estimation algorithm and battery model can be easily implemented on an embedded system using Model-Based Design (MBD).

The scope of this paper focuses on how the DFN battery model is implemented in COMSOL Multiphysics, how the most sensitive model parameters are classified using QR decomposition with column pivoting and how the model parameters for a commercial lithium-ion battery are identified performing microstructure analysis, time-domain characterization and model optimization. The model is validated with Constant Current (CC) and highly dynamic drive cycles. Finally, the DFN model is used to validate the simplifications made on the model which is intended for implementation on an embedded system for real-time state estimation using appropriate algorithms.

Theory

The Doyle-Fuller-Newman (DFN) model is a full order electrochemical cell model based on porous electrode and concentrated solution theories. This model was developed in the 1990s by Doyle, Fuller and Newman and it is also known as pseudo-2D (P2D) battery model [3, 4]. It describes the electrochemical process inside the cell according to coupled partial differential equations, ordinary differential equations and algebraic equations. The model describes the transport of lithium-ions due to diffusion in the solid and liquid phase. The charge conservation in both electrodes is described by Ohm's law. The model is divided as shown in Figure 1 into four parts: the two porous electrodes (anode and cathode), the separator and the electrolyte. Lithium can exist in two phases: in the solid phase namely the coated electrode material (anode and cathode) and in the liquid phase if the lithium is dissolved in the electrolyte. The model state variables are as follows:

- Concentration of lithium in the solid phase $c_s(x,r,t)$
- Concentration of lithium in the electrolyte $c_e(x,t)$
- Electric potential in the solid phase $\phi_s(x,t)$
- Electric potential in the electrolyte $\phi_e(x,t)$
- Flux density between solid phase and electrolyte $j(x,t)$

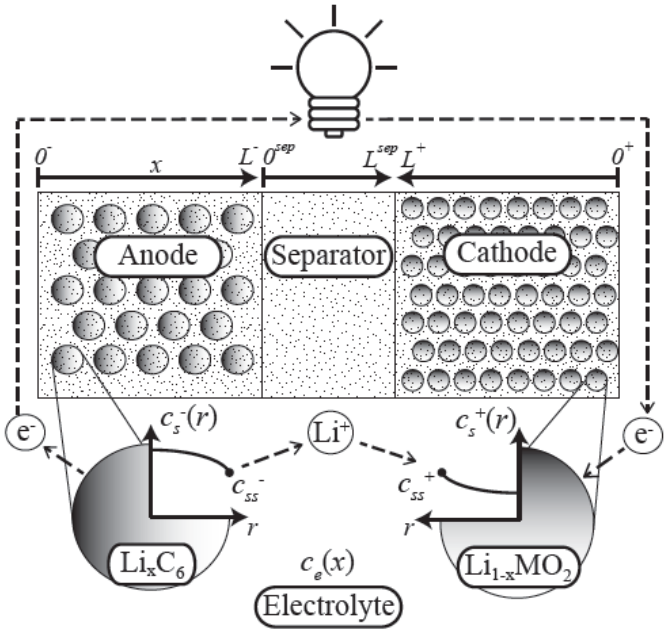

Figure 1: Schematic of the pseudo-2D (P2D) model [9]

Experimental Setup

To characterize the lithium-ion batteries a test setup consisting of a cell tester (ACT0550 from PEC) and a temperature chamber (VT4004 from Vötsch) is used as shown in Figure 2. The cells to be tested are connected with a 4-wires cell holder to the cell tester and installed in a temperature chamber to control the ambient cell temperature.

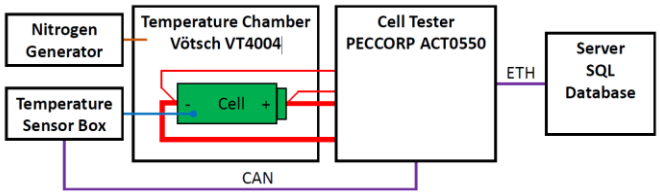

Figure 2: Experimental setup consisting of a cell tester and a temperature chamber for testing the lithium-ion batteries

Governing Equations and Boundary Conditions

Charge Conservation in the Homogeneous Solid

The potential in the solid phase is given by the conservation of charge.

$$\frac{\partial}{\partial x}\left(\sigma^{\text{eff}}\frac{\partial \Phi_s(x,t)}{\partial x}\right) - a_s F j(x,t) = 0 \qquad (1)$$

with the boundary conditions

$$-\sigma^{\text{eff}}\frac{\partial \Phi_s(0^-,t)}{\partial x} = \sigma^{\text{eff}}\frac{\partial \Phi_s(0^+,t)}{\partial x} = \frac{I}{A} = i_{\text{app}}(t)$$

Mass Conservation in the Homogeneous Solid

The diffusion of lithium in the solid electrode particles can be described according to the mass conservation equation governed by Fick's law.

$$\frac{\partial c_s(x,r,t)}{\partial t} = \frac{D_s}{r^2}\frac{\partial}{\partial r}\left(r^2\frac{\partial c_s(x,r,t)}{\partial r}\right) \qquad (2)$$

with the boundary conditions

$$D_s\frac{\partial c_s(x,0^-,t)}{\partial r} = 0 \quad \text{and} \quad D_s\frac{\partial c_s(x,0^+,t)}{\partial r} = -j(x,t)$$

The initial concentration of lithium in the solid phase is constant over the particle volume from the bulk to the surface.

$$c_s(x,r,0) = c_{s,0} \quad 0 \le r \le R_s$$

Mass Conservation in the Homogeneous Electrolyte

The concentration of lithium in the liquid phase (electrolyte) is derived based on mass conservation.

$$\varepsilon_e\frac{\partial c_e(x,t)}{\partial t} = \frac{\partial}{\partial x}\left(D_e^{\text{eff}}\frac{\partial c_e(x,t)}{\partial x}\right) + (1-t_+^0)a_s j(x,t) \qquad (3)$$

with the boundary conditions

$$\frac{\partial c_e(0^-,t)}{\partial x} = \frac{\partial c_e(0^+,t)}{\partial x} = 0$$

The initial concentration of lithium in the liquid phase (electrolyte) is constant over the cross-sectional distance x.

$$c_e(x,0) = c_{e,0}, \quad 0^- \le x \le 0^+$$

Charge Conservation in the Homogeneous Electrolyte
The potential in the liquid phase (electrolyte) is given by the conservation of charge.

$$\frac{\partial}{\partial x}\left(\kappa^{\text{eff}}\frac{\partial \Phi_e(x,t)}{\partial x}\right)+\frac{\partial}{\partial x}\left(\kappa_D^{\text{eff}}\frac{\partial \ln\left(c_e(x,t)\right)}{\partial x}\right) +a_s F j(x,t)=0 \quad (4)$$

The effective diffusional electrolyte conductivity is derived from concentrated solution theory where

$$\kappa^{\text{eff}}=\kappa\varepsilon_e^{\text{brug}}$$

$$\kappa_D^{\text{eff}}=\frac{2RT}{F}\kappa^{\text{eff}}(t_+^0-1)\left(1+\frac{\mathrm{d}\ln(f_\pm)}{\mathrm{d}\ln\left(c_e(x,t)\right)}\right)$$

with the boundary conditions

$$\frac{\partial c_e(0^-,t)}{\partial x}=\frac{\partial c_e(0^+,t)}{\partial x}=0$$

Lithium Movement between the Solid and Liquid Phases
The Butler-Volmer equation describes the molar flux in function of concentration of lithium in the solid and electrolyte.

$$j=k_0 c_e^{1-\alpha}\left(c_{s,\max}-c_{s,e}\right)^{1-\alpha}c_{s,e}^{\alpha}\left(\exp\left(\frac{(1-\alpha)F}{RT}\eta\right) -\exp\left(-\frac{\alpha F}{RT}\eta\right)\right) \quad (5)$$

The overpotential is defined as

$$\eta=\Phi_s-\Phi_e-U_{\text{OCP}}-jFR_{\text{film}}$$

The terminal voltage is calculated by the potential difference between the two current collectors minus the voltage drop over the film resistance.

$$v(t)=\Phi_s(0^+,t)-\Phi_s(0^-,t)-\frac{R_f}{A}i_{\text{app}}(t)$$

Summarization of the Governing Equations
The equations 1, 2, 3, 4 and 5 together with the Open Circuit Potential (OCP) model comprise the Doyle-Fuller-Newman (DFN) or pseudo-2D battery model. Applying these equations to the two electrodes and the separators results in a large and computationally demanding model. The states of the liquid phase evolve in x direction and for the solid phase in x and r direction.

Model Implementation

COMSOL Multiphysics and the Batteries & Fuel Cells Module is used to solve the model in time and frequency domain. The model mainly consists of the two porous electrodes, the separator and the electrolyte as shown in Figure 3. Within the porous electrode model, the particle intercalation and the porous electrode reactions are described.

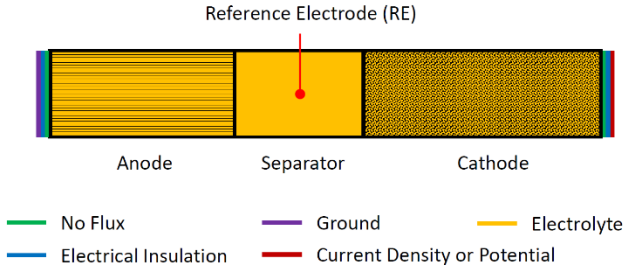

Figure 3: Model implementation in COMSOL Multiphysics

A dedicated powerful server with Linux as operating system running COMSOL Server is used to solve the model efficiently. COMSOL LiveLink for Matlab is used to interact from Matlab with the COMSOL environment, enabling the usage of the MathWorks Optimization Toolbox for parameter identification.

Parameter Identification

The model parameters are identified for a commercial 3.5Ah 18650 nickel-rich, silicon-graphite lithium ion battery.

Parameter Grouping and Sensitivity Analysis
Based on literature review and best practices the parameters of the DFN cell model are first grouped into geometric, thermodynamic and kinetic parameters. All geometrical parameters can be identified by opening the cell and performing a microstructure analysis. The thermodynamic parameter group describes the cell voltage at equilibrium. Those parameters can be determined by low current tests to minimize the dynamic characteristics of the cell. All other parameters, that are not classified as geometric or thermodynamic parameters, are classified as kinetic parameters. These parameters are not easy to identify by measurements. A simple approach to identify them can be achieved by model optimization using recorded pulse pattern battery test data from the laboratory.
During the sensitivity analysis the parameters from similar cells described in literature are normalized linear if the parameter range is within the same magnitude and logarithmic for parameters of different order of magnitudes.

$$p_i=\beta\min(p_i)+(1-\beta)\max(p_i)$$

$$\log(p_i)=\beta\log\left(\min(p_i)\right)+(1-\beta)\log\left(\max(p_i)\right)$$

Individual parameters are varied by setting β to an arbitrary value within the interval [0, 1] while remaining β for the other parameters at 0.5. The most sensitive kinetic model parameters are classified by QR decomposition with column pivoting [10]. The DFN model for the analysis is expressed as follows:

$$\boldsymbol{v}(t)=h\left(\boldsymbol{i}_{\text{app}}(t),\boldsymbol{p},\boldsymbol{c}_{e,0}\right)$$

The first order Taylor series expansion for the model output around the nominal parameters $\boldsymbol{p}_{\text{nom}}$ is expressed as:

$$\boldsymbol{v}(\boldsymbol{p}_{\text{nom}}) = \boldsymbol{v}(\boldsymbol{p}) + \frac{\partial \boldsymbol{v}}{\partial \boldsymbol{p}_{\text{nom}}}\Big|_{\boldsymbol{p}} (\boldsymbol{p}_{\text{nom}} - \boldsymbol{p})$$

Thereby, the sensitivity matrix $\boldsymbol{S} = \frac{\partial \boldsymbol{v}}{\partial \boldsymbol{p}_{\text{nom}}}$ has the size N by m. Where N is the number of measurements of the applied current $\boldsymbol{i}_{\text{app}}(t)$ and m is the number of dynamic parameters $\boldsymbol{p}$. Since the parameters in $\boldsymbol{p}$ have different magnitudes the sensitivity matrix is normalized by the nominal parameter $\boldsymbol{p}_{\text{nom}}$ where $\boldsymbol{\Gamma_0}$ is equal to the diagonal matrix of $\boldsymbol{p}_{\text{nom}}$.

$$\boldsymbol{S}(\boldsymbol{p}, \boldsymbol{t})_{\text{nom}} = \boldsymbol{S}(\boldsymbol{p}, \boldsymbol{t})\boldsymbol{\Gamma_0}$$

Next the QR decomposition on the normalized sensitivity matrix is performed to determine the orthogonal matrix $\boldsymbol{Q}$, the upper triangular matrix $\boldsymbol{R}$ and the permutation matrix $\boldsymbol{\Pi}$ such that $\boldsymbol{S}(\boldsymbol{p}, \boldsymbol{t})_{\text{nom}}\boldsymbol{\Pi} = \boldsymbol{QR}$. Thus, the permutation matrix can be used to resort the dynamic parameter index according to the most sensitive order.

$$\text{index}(\boldsymbol{p})_{\text{most sensitive}} = \text{index}(\boldsymbol{p})\boldsymbol{\Pi}$$

Finally, the most sensitive kinetic model parameters are selected for identification.

Microstructure Analysis

For the microstructure analysis two new batteries are selected. First, they are deep discharged to ensure that no energy is left in the cell and they can be opened safely without leading to a fire and damage the surrounding. The first battery is opened by removing the metal case and unrolling the rolled layers to measure the active coated area. The second battery is cut axially into small samples and impregnated with resin under vacuum to preserve the internal structure. Then, the cut surface is grinded and polished subsequently for further analysis.

The thickness of the individual layers is determined at different positions with the optical microscope. The active volume fraction and porosity are determined by scanning electron microscopy (SEM) and subsequent image processing using Otsu's multilevel thresholding method. The particles are detected by searching the ridge lines by computing the Skeleton by Influence Zones (SKIZ). For each found object the watershed segmentation algorithm is applied to find the most likely local particle boundaries. The particle radius is then calculated based on the particle area given by the boundaries as shown in Figure 4.

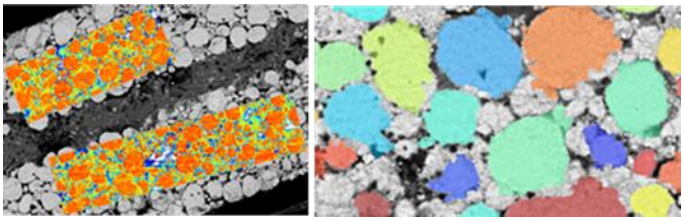

Figure 4: Microstructure analysis applying image processing on the SEM image to determine the particle radius

Energy Dispersive X-ray spectroscopy (EDX) is performed to determine the composition of the coated material, which in turn is used to take OCP measurements from the literature.

Thermodynamic Parameters

To identify the thermodynamic parameters the stoichiometry fraction of the OCP measurements for anode and cathode are determined based on Open Circuit Voltage (OCV) measurements performed on cell level. The stoichiometry fraction can be determined by defining the optimization problem given in Equation 6 and solved with the Levenberg-Marquardt algorithm and initial conditions in the range [0, 1].

$$\boldsymbol{\theta}^* = \min_{\boldsymbol{\theta}} \left(\begin{bmatrix} U^{cell}_{\text{OCV,dsg}} - \widehat{U}^{\text{cell}}_{\text{OCV,dsg}} \\ U^{cell}_{\text{OCV,chg}} - \widehat{U}^{\text{cell}}_{\text{OCV,chg}} \end{bmatrix} \right)^2 \tag{6}$$

$$\widehat{U}^{\text{cell}}_{\text{OCV}} = U^{\text{pos}}_{\text{OCP}}(y_{0\%}, y_{100\%}, z) - U^{\text{neg}}_{\text{OCP}}(x_{0\%}, x_{100\%}, z)$$

The OCV of the cell is determined in the laboratory by applying an improved method of the Galvanostatic Intermittent Titration Technique (GITT) test. In this case the switching condition for the end of a relaxation pulse is based on the voltage gradient at equilibrium (20uV min^{-1}) and not on a fixed time according to the standard procedure. The model validation of the thermodynamic parameters is shown in Figure 5, within 100% to 5% SOC, the OCV model error remains within 10mV.

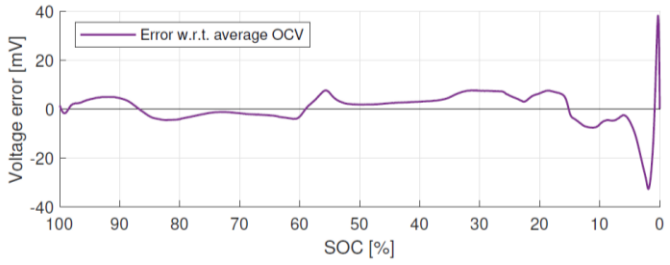

Figure 5: Cross-validation of the OCV model with average 0.05C CC OCV measurements

Kinetic Parameters

The dynamic parameters are identified by a multi-objective optimization problem with shared parameters $\boldsymbol{p}$ as shown in Equation 7. Each function $f_i\left(\boldsymbol{p}, I_{i,\text{app}}(t)\right)$ describes the error between the simulated cell voltage from the COMSOL model and the measured voltage on the real cell by applying a current profile $I_{i,\text{app}}(t)$.

$$\boldsymbol{p}^* = \min_{\boldsymbol{p}} \left(\begin{bmatrix} f_1\left(\boldsymbol{p}, I_{1,\text{app}}(t)\right) \\ f_2\left(\boldsymbol{p}, I_{2,\text{app}}(t)\right) \\ \vdots \\ f_n\left(\boldsymbol{p}, I_{n,\text{app}}(t)\right) \end{bmatrix} \right)^2 \tag{7}$$

$$f_i\left(\boldsymbol{p}, I_{i,\text{app}}(t)\right) = U_{\text{model}}\left(\boldsymbol{p}, I_{i,\text{app}}(t)\right) - U_{\text{cell}}\left(\boldsymbol{p}, I_{i,\text{app}}(t)\right)$$

The optimization problem is solved by nonlinear least-squares regression technique based on trust region as shown in Figure 6. The optimization routine is performed in Matlab and the model is solved in COMSOL Multiphysics using LiveLink.

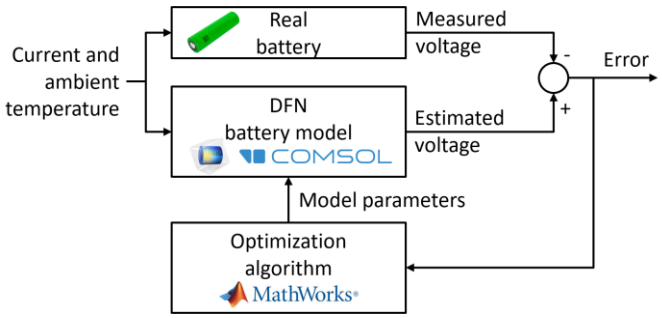

Figure 6: Method for the dynamic parameter optimization using COMSOL Multiphysics, Matlab and LiveLink

Model Validation

The DFN model is validated by applying CC discharge tests and dynamic drive cycles. Figure 7 shows the model performance for CC discharges with different C-rates. The simulated cell voltage is in line with the measured ones.

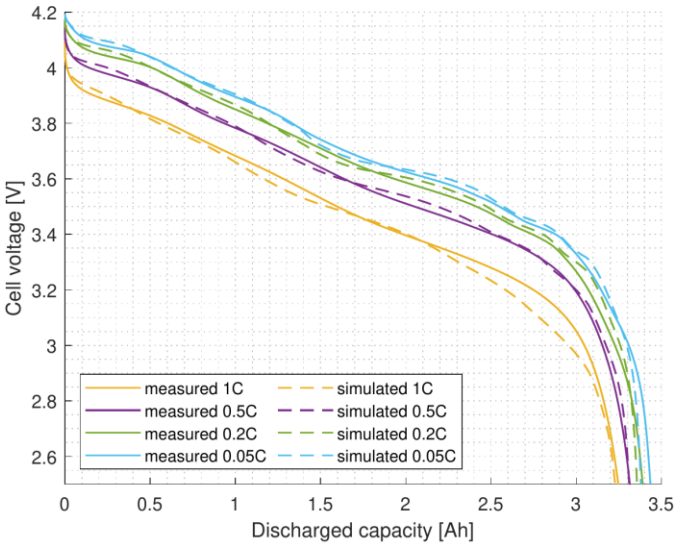

Figure 7: DFN model validation by CC discharge tests

Four standardized drive cycles (HWFET, NYCC, UDDS and US06) are used to validate the model with realistic drive cycles as they occur in EVs. A model of an EV is used to obtain the current profile on cell level according to the speed profile from the mentioned drive cycles. Moreover, the current profiles are grouped and consecutively scaled to 2C and 5C for the highest discharge current peak. Table 1 shows the RMSE of the cross-validation for different initial SOCs. Within 90% to 20% SOC the average RMSE is 11.4mV, at low SOC (10%) the error increases significantly, the overall average RMSE is 17.3mV.

Drive Cycle	C-rate [C]	SOC [%]								
		90	80	70	60	50	40	30	20	10
HWFET	2C	7.5	11.2	12.2	17.2	4.7	13.8	6.7	13.8	64.5
NYCC	2C	1.7	2.3	2.6	4.0	1.6	3.4	0.9	2.6	13.1
UDDS	2C	6.1	6.8	6.9	17.9	3.0	8.6	4.1	12.1	52.3
US06	2C	10.5	15.5	16.8	15.9	7.1	17.1	7.9	14.8	74.3
HWFET	5C	6.3	26.0	15.7	8.9	19.1	24.4	8.9	13.5	142.9
NYCC	5C	4.3	5.4	7.1	11.8	2.5	7.2	2.8	6.9	33.8
UDDS	5C	18.1	16.0	12.9	11.2	7.9	17.2	11.9	16.2	95.0
US06	5C	21.7	27.9	15.8	9.2	37.1	21.7	10.3	23.8	43.5

Table 1: Cross-validation of the DFN model according to standardized drive cycles (HWFET, NYCC, UDDS and US06)

Figure 8 shows the model performance for the UDDS drive cycle scaled to 5C at 70% initial SOC. The simulated cell voltage agrees well the measured voltage over the entire test duration, the RMSE in this case is 12.9mV.

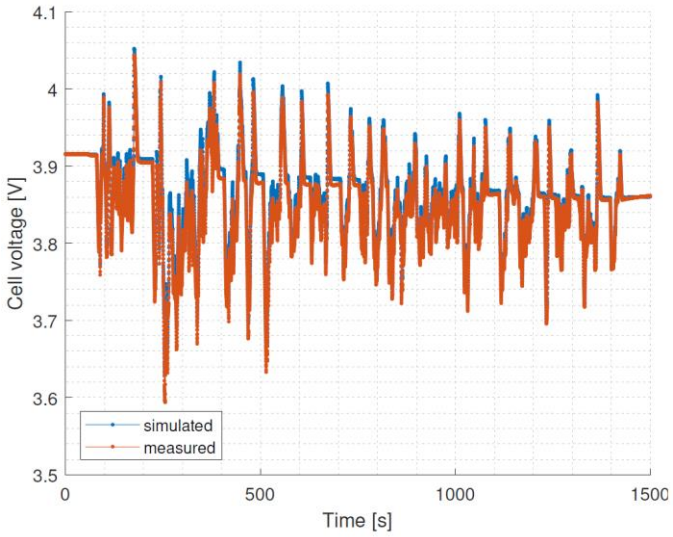

Figure 8: Model performance of the UDDS drive cycle at 70% SOC and current scaling to 5C for the maximum peak within all cycles

Simulation Results

In this section, the simulation results of the electrochemical state variables of the DFN model and the identified parameters from the real cell are presented. For simplicity and better interpretability, the simulation for the 1C CC discharge cycle is considered in function of position and time respective SOC. In the following illustrations, the sequence of layers along the x-axis from left to right is anode, separator and cathode.
Figure 9 shows the potential in the solid phase. Because the active material is highly conductive the potential within the same electrode remains almost constant along the layer thickness. No solid phase potential can be observed in the separator as it does not contain any solid conductive material. The simulated cell voltage from Figure 7 is the difference between the solid phase potential on the far right and left.

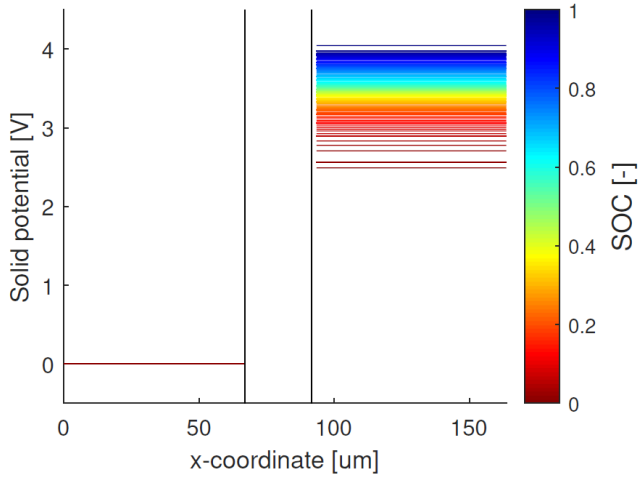

Figure 9: Solid phase potential in function of position and SOC for a complete 1C CC discharge cycle

Figure 10 shows the liquid phase (electrolyte) potential. During discharge, the potential in the anode is expected to increase slowly across the layer and for the cathode, the potential should gradually converge to a stable value. Furthermore, the slope of the potential at the current collectors should be zero. These two assumptions are fulfilled as shown in Figure 10. Within the separator the potential has a linear slope.

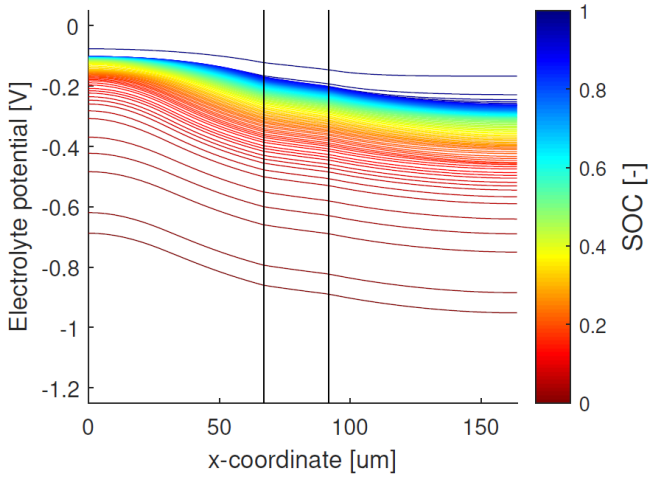

Figure 10: Liquid phase (electrolyte) potential in function of position and SOC for a complete 1C CC discharge cycle

The liquid phase (electrolyte) salt concentration is depicted in Figure 11. For this model the initial salt concentration is set to 2000 mol m^{-3}. The concentration of electrolyte over the simulation time must be conserved. The salt concentration is more unevenly distributed towards the end of discharge especially in the anode.

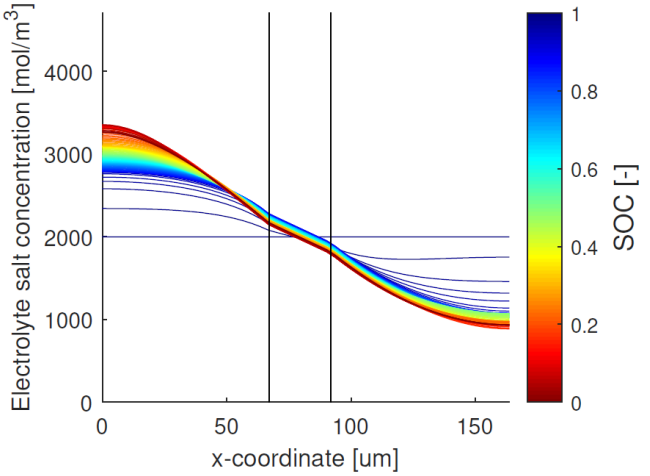

Figure 11: Liquid phase (electrolyte) salt concentration in function of position and SOC for a complete 1C CC discharge cycle

Furthermore, the Full Order Model (FOM) is used to validate the accuracy of Reduced Order Models (ROM) that are suitable for implementation on an embedded system. For the subsequent simulation the DFN is simplified to the SPM that approximates the solid phase of each electrode with a single spherical particle. The PDEs of the SPM are reduced to Ordinary Differential Equations (ODE) assuming polynomial lithium concentration in the particle [5] and applying volume-averaged methods to the solid and liquid phase to preserve the electrolyte dynamics [7, 8]. For demonstration of the model accuracy, a 1C CC charge pulse for 10min followed by a 0.5C CC discharge pulse for 20min is simulated.
Figure 12 shows a minimal cell voltage error of the SPM compared to the DFN during the dynamic phase, while the equilibrium voltage at the end of the simulation is equal.

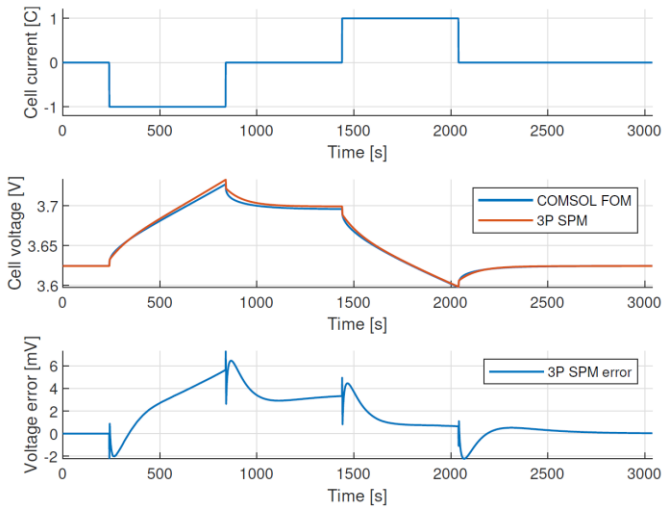

Figure 12: Simulation of the DFN and SPM cell voltage

To investigate the reason of the voltage deviation between DFN and SPM, the electrochemical state variables are analyzed in detail. Figure 13 shows the simulation error between the DFN and SPM volume averaged lithium concentration in the solid

phase. The simulation shows a minimal deviation when the cell is charged to a different SOC.

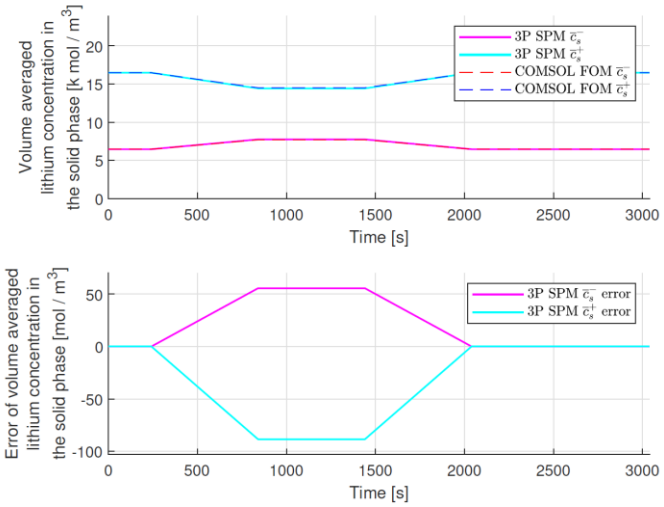

Figure 13: Simulation of the DFN and SPM volume averaged lithium concentration in the solid phase

The error of lithium concentration in Figure 14 shows a significant difference between the DFN and the SPM model. With this simulation it can be concluded that the simplification of the electrolyte dynamics can be further improved.

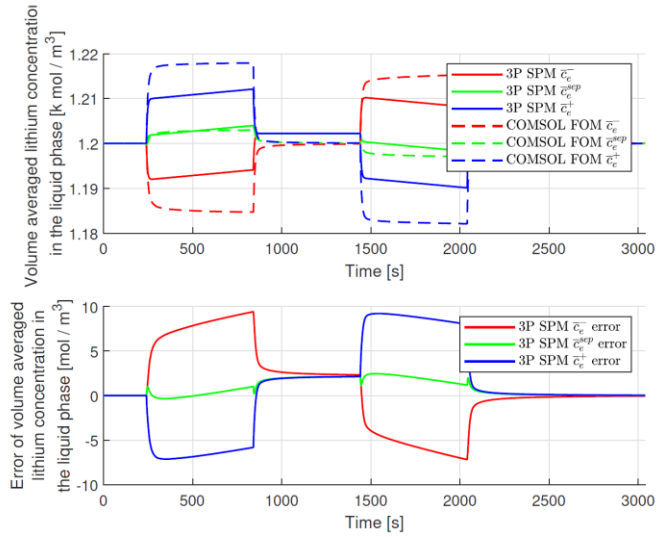

Figure 14: Simulation of the DFN and SPM volume averaged lithium concentration in the liquid phase (electrolyte)

Conclusions

Batteries are used in many applications in our modern world, enabling the seamless transition to a decarbonized mobility and power generation. Many of these applications need to use several cells requiring advanced BMSs for safe operation and maintenance of availability under various load conditions. By using physics-based battery models, the electrochemical cell internal states can be estimated on the BMS using optimal state estimation algorithms enabling degradation minimization strategies and fast charging. In this paper the pseudo-2D DFN battery model is implemented in COMSOL Multiphysics using the Batteries & Fuel Cells Module. A three-step parameter identification approach was developed and applied to identify the DFN parameters for a commercial lithium-ion battery. This procedure encompasses microstructure analysis to determine the geometric parameters, cell tests at equilibrium to identify the thermodynamic parameters by optimization and current pulse patterns to determine the kinetic parameters. The complete model was cross validated with realistic drive cycle revealing an output voltage error smaller than on average 18mV over the full SOC range. This is comparable to literature and therefore, it is concluded that the method presented in this paper is suitable for parameter identification of lithium-ion batteries. Finally, the DFN model is used to validate the simulated electrochemical states of a SPM with electrolyte dynamics suitable for implementation on an embedded system (BMS). The validation reveals that the ROM lithium concentration in the liquid phase does not match the FOM simulation and needs to be improved.

References

[1] Energiespeicher-Monitoring 2018 Leitmarkt- und Leitanbieterstudie: Lithium-Ionen-Batterien für die Elektromobilität, *Fraunhofer ISI*, (2018)

[2] Gregory L. Plett, Battery Management Systems, Volume II: Equivalent-Circuit Methods, *Artech House*, (2015)

[3] Doyle et al., Modeling of Galvanostatic Charge and Discharge of the Lithium/Polymer/Insertion Cell, *Journal of the Electrochemical Society*, 140(6), 1-36, (1993)

[4] Fuller et al., Simulation and Optimization of the Dual Lithium Ion Insertion Cell, *Journal of The Electrochemical Society*, 141(1), 1-6, (1994)

[5] Subramanian et al., Efficient Macro-Micro Scale Coupled Modeling of Batteries, *Journal of The Electrochemical Society*, 152(10), A2002-A2008, (2005)

[6] Tran et al., Matlab Simulation of Lithium Ion Cell Using Electrochemical Single Particle Model, *IEEE 2nd Annual Southern Power Electronics Conference (SPEC)*, 1-6, (2016)

[7] Kemper and Kum, Extended Single Particle Model of Li-Ion Batteries Towards High Current Applications, *IEEE Vehicle Power and Propulsion Conference*, 158-163, (2013)

[8] Lee et al., One-dimensional physics-based reduced-order model of lithium-ion dynamics, *Journal of Power Sources*, 220, 430-448, (2012)

[9] Thomas et al., Advances in Lithium-Ion Batteries: Mathematical Modeling of Lithium Batteries, *Springer-Verlag*, New York, (2002)

[10] Jin et al., Parameter Estimation of an Electrochemistry-based Lithium-ion Battery Model using a Two-Step Procedure and a Parameter Sensitivity Analysis, *International Journal of Energy Research*, 42(7), 2417-2430, (2018)

Nomenclature

Latin symbols

A	Surface electrode area	m^2
a_s	Active surface area per electrode unit volume	$m^2\ m^{-3}$
c	Concentration of lithium	$mol\ m^{-3}$
$c_{e,0}$	Steady-state concentration of lithium in the liquid phase	$mol\ m^{-3}$
$c_{s,0}$	Initial concentration of lithium in the solid phase	$mol\ m^{-3}$
D_e^{eff}	Effective electrolyte diffusivity	$m^2\ s^{-1}$
D_s	Solid diffusivity	$m^2\ s^{-1}$
$f_{\pm}$	Mean molar activity coefficient	-
F	Faraday's constant	96487 $C\ mol^{-1}$
I	Applied current	A
i_{app}	Applied current density	$A\ m^{-2}$
j	Molar ion flux	$mol\ m^{-2}\ s^{-1}$
r	Radial coordinate in solid particle	m
R	Universal gas constant	8.31451 $J\ mol^{-1}\ K^{-1}$
R_{film}	Film resistance	$\Omega\ m^2$
R_s	Particle radius	m
t	Time	s
t_+^0	Transference number of Li^+	-
T	Temperature	K
U	Voltage	V
v	Cell voltage	V
x	1D cross-sectional coordinate	m
z	State of charge (SOC)	-

Greek symbols

α	Charge transference coefficient	-
ε	Volume fraction	-
η	Electrical Overpotential	V
κ^{eff}	Effective electrolyte conductivity	$S\ m^{-1}$
σ^{eff}	Effective solid conductivity	$S\ m^{-1}$
Φ	Electrical Potential	V

Subscript/superscript

e	Liquid phase (i.e. electrolyte)
eff	Transport corrected (Bruggeman correlation)
neg	Negative electrode (i.e. anode)
pos	Positive electrode (i.e. cathode)
OCP	Open circuit potential (half-cell level)
OCV	Open circuit voltage (cell level)
s	Solid phase (i.e. active particle)